Published version at: https://doi.org/10.1016/j.clay.2020.105736

Determination of uranium and thorium isotopes in kaolinitic samples by ICP-MS/MS

J.L. Mas[1], P. Aparicio[2], E. Galán[2], A. Romero-Baena[2], A. Miras[2], A. Yuste[3] D. Martín[2].

1: Dpto. Física Aplicada I, Escuela Técnica Superior de Ingeniería Informática, Avda. Reina Mercedes s/n, Universidad de Sevilla. 41012 Sevilla (Spain).

2: Dpto. Cristalografía, Mineralogía y Química Agrícola, Facultad de. Química, Avda. Reina Mercedes s/n, Universidad de Sevilla. 41012 Sevilla (Spain).

3: Dpto. Ciencias de la Tierra, Facultad de Ciencias, Calle Pedro Cerbuna, 12, Universidad de Zaragoza. 50009 Zaragoza (Spain).

Abstract.

The use of natural uranium and thorium long-lived isotopes was applied to study the evolution of kaolinitic materials. To do that, a radiochemical method for separation of Th and U in phyllosilicate samples was developed with the main aim of their analysis by ICP-MS/MS. Given the lack of certified phyllosilicate reference materials with certified isotope abundances, the method was tested using a stepwise approach. First, a preliminary setup was done using a sediment reference sample. Then, the extrapolation of this method to the samples of interest has been tested using a phyllosilicate sample certified for U and Th concentrations. The results showed that an extension of the plateau time of digestion in the used microwave system was peremptory as to get full digestion of the sample. The use of the isotope dilution technique allowed both the quantification of major isotopes (^{238}U and ^{232}Th) simultaneous to the determination of isotope ratios ($^{234}U/^{238}U$, $^{235}U/^{238}U$ for quality control and $^{230}Th/^{232}Th$). The established method was applied to six kaolinitic samples from the Iberian Range (NE Spain), showing the potential of this isotope approach for the characterization of their time evolution.

Keywords: Kaolinitic materials, Isotopic analysis, Uranium and Thorium Isotopic ratio; Recent time evolution

1. Introduction.

The association of phyllosilicates in continental sedimentary deposits can provide important insights about the paleoclimate and weathering conditions where they formed (Ruffell et al., 2002; Raucsik and Varga, 2008). However, continental sedimentary rocks usually include different kinds of phyllosilicates, a fact that makes difficult the interpretation of their study: detrital phyllosilicates, mainly associated with the composition and weathering conditions in the source area, authigenic phyllosilicates

providing information about syn-sedimentary conditions in the environment, and diagenetic phyllosilicates being generated during sediment consolidation through a series of processes that could introduce severe perturbation of the paleoclimate signal. Once these effects have been taken into account, clays minerals can be used as proxies for humidity conditions in Tertiary and Mesozoic sedimentary records (Ruffell et al., 2002; Pellenard and Deconinck, 2006).

The relative proportions between kaolinite and smectites can be used as indicators of the role of chemical weathering: for smectites, there are already described relationships between chemical composition and environmental conditions (ÇIflikli et al., 2013; Dill, 2017). However, the major chemical composition of kaolin minerals is independent of their origin. Therefore, kaolinitic samples have been extensively studied from a geochemical point of view, including analyses for major and trace elements such as REEs, uranium and thorium concentrations (Fernández-Caliani et al., 2010; Galán et al., 2016), stable isotopes (Clauer et al., 2015), etc. It is worthy to note, however, that no attention has been paid to the relationships between the different naturally occurring isotopes of uranium and thorium.

^{238}U ($T_{1/2}=4.47\cdot10^{9}$ y) and ^{234}U ($T_{1/2}=2.46\cdot10^{5}$ y) belongs to the same radioactive series. It is expected that within a closed system isolated from weathering, the initial ^{234}U content decays to a proportion of less than 0.40 % within eight half-lives of the grand-daughter. Due to the disintegration of the grand-parent, the application of the Bateman's equations allows to conclude that both isotopes should reach near secular equilibrium in six half-lives of the grand-daughter. Under these circumstances, it is expected that the initial proportion between isotopes of uranium at the time of formation is lost and completely replaced by the establishment of a secular equilibrium condition after just $<2\cdot10^{6}$ y. In this way, deviations of isotope ratios from the secular equilibrium value should reflect the effect of the recent evolution (mainly through weathering) of kaolinitic materials, see e.g., Richland et al. (2003). On the other hand, ^{230}Th ($T_{1/2}=7.54\cdot10^{4}$ y) is produced as a consequence of the disintegration of ^{234}U through several short-lived isotopes, while ^{232}Th ($T_{1/2}=1.40\cdot10^{10}$ y) starts another radioactive chain; therefore $^{232}Th/^{230}Th$ isotope ratios depends not just on the initial contents of the sample, but also on its subsequent evolution.

Several works in the literature have dealt with the concentrations of certain natural radioisotopes in kaolinitic samples from the point of view of its radiological impact (El-Dine et al., 2004), its role on the bioavailability of uranium (Crawford and Liber, 2015) or its relation with uranium mineralization (Beyer et al., 2011). However, no exploration is known on the potential of uranium and thorium isotope ratios to provide further insight into the evolution of kaolinitic materials after their formation. In this case, we should consider a null hypothesis to verify or reject, which is that all the nuclides from the same radioactive series ($^{238}U/^{234}U/^{230}Th$) are in secular equilibrium, while the $^{238}U/^{232}Th$ isotope ratio mimics that of the local continental crust (Masarik, 2009).

A vast amount of methods for the analysis of uranium and thorium isotopes have been published elsewhere, based on radiometric and atom counting techniques (Hou and Roos, 2008). During the last two decades, ICP-MS has received special attention due to a combination of certain analytical advantageous features such as minimization of the sample mass, precision and high sample throughput (Hou and Roos, 2008). The analysis of major uranium and thorium isotopes, which average concentrations in Earth crust are 0.91 and 3.5 ppm, respectively (Taylor and McLenann, 1985), is a routine technique provided a full dissolution of the rock matrix is done (Osmond and Ivanovich, 1992). However, ^{234}U isotope concentrations are in the range of ~$2 \cdot 10^4$ times below that level, while ^{230}Th concentrations are usually 10^4-10^6 times below ^{232}Th concentrations. At these concentration levels, the effect of spectrometric interferences and the lack of precision at very low concentrations preclude the use of the routine "dissolve, dilute and shoot" approach, thus the application of a radiochemical method to extract and isolate both Th and U isotopes from the sample matrix is peremptory.

At Laboratory of radioisotopes, CITIUS, (Univ. Sevilla, Spain), a method was developed for the analysis of trace element concentrations, uranium and thorium isotope ratios by ICP-MS from a single sample aliquot (Mas et al., 2012). However, this method was addressed to the analysis of soil, sediment and NORM sample leachates, but not to the analysis of bulk phyllosilicates: it is expected that these analytes remain partially or completely attached to the refractory sample matrix. On the other hand, recent intercomparing exercises organized by the Spanish Nuclear Safety Council (CSN) revealed high discrepancy of results for analyses of Th in environmental samples (Lozano, 2012). This is the reason why the CSN funded a research project (OPNCSN012/008) devoted to the establishment of a robust method for the determination of Th isotopes in solid samples. Despite the method they proposed included the same central step of the method referred above (separation of uranium and thorium using a chromatographic extraction resin Triskem UTEVA® resin), there were very important differences that could potentially affect the effectiveness for U and Th separation. Indeed, the special characteristics of phyllosilicates establish important restrictions on sample pre-treatment; the ways used to overcome such restrictions or limitations affects in turn the performance of the methodology.

The main aims of this work are: a) establishing the chemical fractionation of uranium and thorium throughout the general method proposed by (Herranz et al., 2015) as adapted for measurement using tandem quadrupole ICP-MS/MS, b) testing the possibilities of the analyses of uranium and thorium isotopes in kaolinitic samples.

2. Materials and methods.

2.1. Sample description.

To the best of our knowledge, there are no certified reference materials of kaolinitic matrices having an isotopic composition for uranium and thorium. Therefore, the radiochemical setup and the method performances were tested using a stepwise approach and involving two reference samples. During an initial stage, the IAEA-385

certified reference material (CRM) was used to test the element fractionation during the radiochemical separation. Uranium and thorium isotopes mass activities are certified for this sample (Pham et al., 2008). This sediment sample has a very low N and organic C contents (0.13 and 0.95%, respectively) for the total carbon content of 2.75%. The main elements are Si (16%), Ca (5.5%), Al (4.5%), Fe (3.1%) and K (1.8%) (Pham et al., 2005). Of course, this sample is not a kaolinitic sample, but it gives the analyst the advantage of using a well-known CRM having certificate information enough as to test the robustness of the calculated isotope ratios. Bearing in mind the nature of this CRM, it is expected that its digestion is much easier than for kaolinitic samples. Therefore, a second CRM was used to test how valid the previously established method could be extended to phyllosilicate samples. In this case, IAG DBC-1 ball clay was used. Isotope ratios are not certified, but uranium and thorium element concentrations are.

The studied samples were collected from different outcrops (Fig. 1) located in the easternmost part of the Iberian Range (NE Spain), the so-called linking zone between the Catalonian Coastal Range and the Iberian Range, or Maestrazgo Basin. This basin was originated during one of the most active stages of the Late Jurassic-Early Cretaceous rifting process (Salas and Casas, 1993; Van Wees et al., 1998) related to the spread of the Tethys westwards and the opening of the Atlantic Ocean, which generated the Iberian Basin and controlled the accumulation of Late Palaeozoic and (mainly) Mesozoic sediments. In the Maestrazgo Basin, the sedimentary filling exceeds 4000 m thick and is characterized by the predominance of shallow marine carbonate sediments interrupted by widespread clastic systems during the Lower Aptian and the Albian (Lower Cretaceous). Nevertheless, terrigenous siliciclastic sedimentation dominated in the western basin margin during the Upper Jurassic-Middle Barremian, represented by Purbeck and Weald facies (Salas, 1989; Salas et al., 1995).

During the Upper Cretaceous, the Alpine orogeny took place with the convergence between European, Iberian and African plates (Casas Sainz and Faccena, 2001). Consequently, the Iberian basin became compartmentalized (García and Mas, 2004) and the beginning of emergence started in some zones (Mas, 1981; Carenas, 1987; Martin-Chivelet et al., 2002). Subsequently, during Eocene to early late Oligocene times, the Catalonian-Valencia Basin and, in early Miocene, the Iberian Basin were inverted to form the Iberian Range and the Catalonian Coastal Range (Salas et al., 2001). Recently, the Iberian Range experienced a regional uplift since the Late Pliocene (~3 Ma) with a maximum in the Maestrazgo zone (Giachetta et al., 2015).

Sample F2Y comes from the Lower Cretaceous (Barremian) Fuentespalda karst bauxite deposit (Teruel). The deposit consists of pisolitic bauxite and clays infilling karst cavities developed in Upper Oxfordian-Kimmeridgian limestones and argillaceous limestones. As a consequence of karst reactivation, they show heterogeneous chaotic lithostructure (Bardossy, 1982) consisting of up to metric-sized pisolitic bauxite blocks embedded in red clays. Pisolitic bauxites are mainly red (as sample F2Y), but white zones are frequently observed in the upper parts of blocks, which is related to late kaolinization processes due to circulation of acid solutions linked to karst reactivation

(Yuste et al., 2015). The paleokarst is overlain by Albian sandstones and/or by Cenomanian dolomitized limestones (Molina and Salas, 1993).

Sample FR9 is a lateritic claystone from the Barremian Artoles Formation (Salas, 1987). This Formation, up to 200 m thick, is a shallow marine carbonate unit made of grey limestones and marls that includes some lateritic clays. It corresponds to a coastal platform environment with little continental sedimentation episodes, characteristic of an estuary environment. The sample comes from an outcrop located on south of Fredes (Castellón) and consists of a 5 m thick lateritic level overlying karstified limestones. The clays are yellowish-brown at the bottom part and red-purple at the upper part, where the sample was taken.

Sample MV36AC corresponds to a red claystone whereas sample MV36AR is a medium to coarse white creamy sandstone. Both belong to the Barremian Camarillas Fm. (Canérot et al. 1982; Salas, 1987) in the Miravete area (Teruel). Along with the underlying Castellar Fm. it forms the Weald facies (Ruiz-Omeñaca et al., 2004; Canudo et al., 2012) which represents an exceptional stratigraphic record of the Early Cretaceous including kaolin-rich clay deposits (Bauluz et al., 2014). The Camarillas Fm., approximately 200 m thick, is made of commonly yellow-brown to white sandstones, and mainly red claystones and siltstones, with minor grey limestones and marls intercalations. The field appearance of claystones and siltstones resembles that of pedogenically modified rocks, such as those described by (Fernández-Caliani and Cantano, 2010) in south-western Spain. The Camarillas Fm. has been traditionally interpreted as corresponding to a shallow continental environment with emersion periods that promoted palaeosols to be developed (Soria, 1997). Recently, Navarrete et al. (2013) suggested a mixed-carbonate siliciclastic back-barrier environment based on sedimentological data from the middle-upper part of this formation.

Finally, samples AR6 and EST2 are dark grey to black claystones from the Albian Escucha Formation (Aguilar, M.J., Ramírez del Pozo, J., 1971) near Ariño and Estercuel (Teruel), respectively. During the Early Albian, sedimentation in the area was typical of a coastal marine environment that evolved into a deltaic and mudflat environment (Escucha Fm.) (González López et al., 2005). The large amount of organic matter deposited into a low-energy environment, along with a high sedimentation rate, favored the preservation of the organic matter resulting in significant coal deposits (Querol et al., 1992). The Escucha Fm. is approximately 200 m thick in the area and characterized by abundant dark claystones with minor siltstones and sandstones. As mentioned above, it includes several lignite beds in its lower member.

2.2. Radiochemical procedure.

The radiochemical method described below was applied to test uranium and thorium fractionation throughout the procedure. To do that, in several of the steps described below we removed a small aliquot of the resulting solution, which was subsequently

diluted into 1% HNO_3 and measured by ICP-MS/MS for ^{238}U and ^{232}Th concentrations. Fractionations and chemical yields were calculated by comparing the obtained element concentration with the certified value (after correcting by the applied dilution factor). For field samples, the used radiochemical scheme was essentially the same excepting a) certain details that are provided below, and b) that just the U and Th fractions were analyzed.

Figure 2 presents a general view of the applied radiochemical separation. The samples were desiccated at 65ºC (for the IAEA-385, 105ºC for the field and DBC-1 samples) to a constant weight; four replicates of 0.25 g d.w. were transferred to polytetrafluoroethylene (PTFE) liners. 2 mL of HNO_3, 2mL of HCl, 9 mL of HF and 2 mL of 30% H_2O_2 were added and the sample/solution mix was left for at least one hour until effervescence (if any) disappeared. In the case of phyllosilicate samples, previous calcination was used instead of using H_2O_2 (Rihs et al., 2017). HNO_3, HCl and HF were double-distillated in three separate Savillex DST-1000 sub-boiling systems; H_2O_2 was analytical grade (Panreac). For field samples, ~ 2.5 ng of ^{236}U (IRMM-3660a) and ~ 100 pg of ^{229}Th (CIEMAT, Madrid, Spain) were added to each replicate to apply the ID-MS technique. After leaving the samples overnight for equilibration of samples and solutions (and eventually, spikes), they were submitted to full digestion using a microwave oven (Milestone ETHOS Plus One). The digestion program started with a two-step ramp until 220ºC was reached (room temperature to 100ºC: 5 min; 100-220ºC: 10 min). Such temperature was kept, initially, for ten minutes. The liners were kept tightly closed until T<40ºC to minimize potential losses of volatile elements. After washing caps with 18 MΩ·cm water (Millipore Integral-3), the solutions were transferred to previously tared 60 mL PFA beakers (Savillex); the walls and bottom of the PTFE liners were thoroughly rinsed with mQ water. The resulting volume solution (which is coded as Solution 1 in Figure 2) was ~30-45 mL.

Solution 1 was evaporated to incipient dryness on a hot plate. The residue was redissolved using 7 mL of HNO_3 while gently rinsing the beaker's walls and then evaporated again. The process of redissolution and evaporation was repeated twice and the residue was finally recovered using 5 mL of HNO_3 (solution 2 in Fig. 2). When required, redissolution was assisted by using an ultrasound bath for 5-10 min. It was expected that successive low-temperature evaporations allow convenient removal of excess of fluorides, hence avoiding the use of post-digestion steps involving boric acid that can interfere the retention of U and Th in the UTEVA® column (Mas et al., 2012). Thereafter, ~3 mg of Fe (in $FeCl_3$ form, Panreac) were added under gentle stirring; after equilibration for 2 hours, pH of the solution was raised to 9 using subsequently 5% and 30% NH_4OH (analytical grade, Panreac), and iron hydroxides precipitation occurred. The stirrer was removed and both phases (supernatant and precipitate) were separated by centrifugation, 15 min, 3000 rpm. The supernatant (solution 3 in Fig. 3) was discarded after weighting. The precipitate was subsequently redissolved by using 5 mL of 3M HNO_3/1M $Al(NO_3)_3$.

Pre-packed cartridges of Triskem UTEVA® resin (2 mL, 50-100 µm mesh sieve) were coupled to 20 mL PP (polypropylene) syringes and connected to a Triskem AC-12 vacuum box working under a pressure gauge of ~ 34 kPa (which transforms into a volume rate ~ 1 drop per second). The resin was prepared with 10 mL of 3M HNO_3/1M $Al(NO_3)_3$ and the sample was passed through it, then the resin was washed with 10 mL of 3M HNO_3 and subsequently exchanged to the chloride form by passing through 5 mL of 9M HCl. The sample eluate, the rinse eluate and the 9M HCl eluate were collected together and coded as Solution 4 (see Fig.2). Thorium was extracted using 20 mL of 5M HCl/0.05M $H_2C_2O_4$ (Oliveira and Carvalho, 2006), uranium was extracted using 20 mL of 0.01M HCl (Mas et al., 2012). The uranium and thorium solutions were directly collected in 30 mL-PFA Savillex beakers, which were subsequently evaporated to incipient dryness on a hot plate and redissolved with ~ 3 mL of temperature room 1% HNO_3 in the case of uranium (Solution 5 in Fig. 2) and with 15 mL of 9M HCl in the case of thorium (Solution 6). Thorium fraction was subsequently purified using a prepacked cartridge of Triskem TEVA column (2 mL, 50-100 µm mesh sieve) coupled to a Triskem PF-R50A prefilter previously conditioned with 10 mL of 9M HCl; the thorium fraction was passed through and collected in a new 30 mL-PFA Savillex beaker, evaporated to almost dryness and recovered with ~ 3mL of 1% HNO_3 (Solution 7 in Fig. 2).

Solutions 1-7 were diluted *off-line* on a v/v basis in 1% HNO_3 by applying different dilution factors using either a CETAC SDS-550 system or, when high concentrations of HF were present in the solution, by pipetting onto a LDPE calibrated volumetric flask.

Determining the concentration of U and Th in a certain working solution (Solutions 1-7) passed through a previous dilution, which required removing from it a certain mass fraction (x). This scheme implied that the amount of available U and Th for subsequent separation was becoming progressively reduced. This fact was taken into account in the determination of the chemical yields, by applying the corresponding correction:

$$c_{\exp ected} = \frac{x m_s c_{0,a}}{V} \quad (1)$$

$c_{expected}$ is the concentration of the analyte that should be expected when a mass m_s of the certified sample having a certified concentration $c_{0,a}$ is analyzed with a chemical yield of 100%, and a mass fraction x of the resulting solution is diluted onto V mL. The true chemical yields (Y, %) were determined by comparing the concentrations found in the diluted solutions with $c_{expected}$, i.e.:

$$Y = 100 \frac{c_{measured}}{c_{\exp ected}} \quad (2)$$

Of course, removing a mass fraction x implies that the next analytical step contains just a proportion 1-x of the analytes, and the corresponding corrections were made for all the calculations. In this way, the chemical yields calculated in this work were not partial

(i.e., specific for that stage of the analytical procedure), but the overall chemical yield obtained until that step. For all the results, the uncertainties were determined by using the GUM-guide.

2.3. Instrumental technique.

All the measurements were done using the same instrument (Agilent 8800 ICP-MS/MS), which works with two independent quadrupole filters and an octopole collision/reaction cell between them. To test the performances of the method, a conventional sample introduction was used (CETAC ASX-520) and inert cones, torch, torch injector, skimmer base and nebulizer (Savillex CFlow-400) were used. The concentrations of ^{238}U and ^{232}Th were measured by external calibration after adapting the U.S.E.P.A. 200.8 method; instrument conditions are summarized in Table 1. The presence of potentially interfering elements see, e.g., (Mas et al., 2012), was also monitored in solutions 5 and 7. For these measurements, the first quadrupole was working just like an ion guide and not as a mass filter. Uranium and thorium isotopes were analyzed in field samples coupling a high-efficiency nebulizer (CETAC Aridus II) to the ICP-MS/MS, conditions are also shown in Table 1. In this case, both quadrupoles worked by filtering the same mass (i.e., the so-called "*on mass*" approach). For isotopic analyses, automatic dead time correction was applied after calibration the same day of measurement; dead time was always in the range of 25 ns. Pulse/Analog correction was done *on line* using Agilent MassHunter© software. Mass bias correction (linear algorithm) was applied off-line after calibration using certified solutions (IRMM-035 and IRMM-056), bracketed between two unknown samples and a blank. Mass 235 for uranium was analyzed as quality control, expecting that the obtained isotope ratio $^{238}U/^{235}U$ agrees with the natural isotope ratio (~138).

3. Results and discussion.

3.1. Performances of the U and Th separation.

The results obtained for Solution 1 (Table 2) show that the sample digestion was complete. However, when the same method was applied to the DBC-1 reference sample, full sample dissolution was not reached. Filtering the resulting solutions, up to 20% of the sample mass remained undigested. It is impossible to assay the nature of these small black grains associated with the refractory matrix. Of course, the sample mass to be dissolved could be minimized, but in this way, higher dilution factors should be introduced, making even more difficult the quantification of minor isotopes. As a contingency solution, the flat top peak of the digestion sequence was increased from 10 to 25 minutes; after that, no mass was detected in the filters. The procedure blank produced low count rates; Table 2 shows the ratio between the count rate obtained in the procedure blank and the average of count rates obtained for the four sample replicates; it is easy to see that for both U and Th they are near zero within the k=1 significance interval. On the other hand, the results obtained for Solution 2 show that no losses were

produced during the successive evaporations and recoveries, which were introduced to exchange the sample matrix and remove the excess of fluorides: the chemical yields obtained for both analytes were essentially the same as those obtained for Solution 1.

For solution 3, it can be seen that up to 7% of the uranium remained in the supernatant solution, either as a consequence of an incomplete attachment to iron hydroxides floc particles or to a certain resuspension during the centrifugation process. It is interesting, however, to note that losses of uranium were not homogeneous, ranging 0.3-7.4%. This finding contrasts to the results obtained for Th (<0.2% remains in the supernatant), which is in agreement with the higher affinity of Th for particulate material (Herranz et al., 2015). In this case, the contribution of the procedure blank was high because the raw count rates were very low. Regarding solution 4, it was expected that both U and Th remained completely retained into the UTEVA resin assuming the loading solution is appropriate (Carter et al., 1999; Lee et al., 2005; Maxwell and Culligan, 2006; Oliveira and Carvalho, 2006). This is what can be seen in Table 2, solution 4, although small losses were produced for uranium (0.1-0.4%) and thorium (0.4-1.9 %). Once again, the contribution of procedure blank was relatively high as the concentrations of U and Th were small.

The results for Solution 5 (Table 2) show high chemical yields for uranium, with a random exception that we cannot explain. It is worthy to note that despite the extremely high-count rates obtained by ICP-MS/MS, the associated relative uncertainties for uranium concentrations (and subsequently, for uranium chemical yields) were unexpectedly high. This relatively large uncertainty could appear because the corresponding measurements were done (for uranium) using the analog detector mode, given the high-count rates there obtained. The pulse/analog mode calibration was performed a long time before this analytical run and required an update. To avoid this type of problem, the following measurement series were done after including in every batch the option for automatic pulse/analog mode calibration, as shown above. On the other hand, just 0.2-0.9 % of thorium was transferred to the uranium fraction, once again with the same exception mentioned above. This level of cross-talk does not establish analytical problems on the measurement of minor isotopes of uranium due to 1) the very low hydrides rate obtained with the Aridus II (see Table 1), 2) the extremely low isotope abundance of deuterium and 3) the extremely low abundance sensitivity obtained when the ICP-MS/MS system works *on-mass*, which is theoretically in the range of 10^{-14} (Ohno et al., 2013; Balcaen et al., 2015).

Solutions 6 and 7 (Table 2) corresponded to the thorium fraction before and after purification using a TEVA resin. Before purification, the level of U cross-talk into the Th fraction was, in this case, reasonably homogeneous (~1%), and it can seem relatively low. For MS-based techniques, U isotopes should introduce a certain overlap on thorium masses (in this case, 229, 230, 232) as a consequence of poor abundance sensitivity. However, it is well known that this effect decreases as the mass difference between the overlapping mass and the overlapped mass increases (Wyse et al., 2001). The closest masses should be hence 234 and 232. Although the range of U/Th ratios in

any sample can vary over more than one order of magnitude, a 1% of the initial mass of uranium in the thorium fraction could introduce an abundance of the 234 ion several orders of magnitude below that of 232. From that point of view, it could be questioned if the purification of thorium is really necessary when applying MS-based techniques for the measurement of U and Th isotopes. On the contrary, these results showed that this purification step can be peremptory when radiometric based techniques such as alpha-particle spectrometry are used, as the alpha emission energies of Th and U isotopes overlap. Regarding thorium chemical yields, these were relatively homogeneous (75-88%), and the contribution of the procedure blank to the count rate was quite satisfactory (~0.1%).

The results for Solution 7 (Th fraction after the purification with TEVA resin) suggest a certain decrease of Th chemical yield in the range of 10%, while still satisfactory (68-82%), and procedure blank contributions < 0.06%. As expected, using a TEVA resin with a high concentration of HCl partially removed U from the solution (Maxwell and Culligan, 2006; Zheng and Yamada, 2006), in such a way that crosstalk decreased from ~ 1% to ~ 0.03%. According to the expected range of uranium and thorium concentrations and the corresponding requirements for maximum permissible crosstalk, the analyst should consider if the purification step with TEVA resin is really required in terms of cost/benefit.

During the application of this procedure to the kaolinitic samples mentioned above, a new aliquot of the certified reference sample was processed; additionally, a replicate of one of the samples was equally prepared to evaluate the reproducibility of the tested methodology. In this way, the isotope ratios ($^{238}U/^{235}U$, $^{238}U/^{234}U$, $^{232}Th/^{230}Th$) and the U and Th concentrations (which were determined through the isotope ratios 238/236 and 232/229, respectively) were tested for both IAEA-385 and IAG DBC-1. The results are summarized (as the measured/expected ratio) in Fig. 3, which shows that the proposed methodology offered good performances in terms of accuracy and reproducibility. As previously mentioned, the DBC-1 CRM is certified for element concentrations of (among other elements) Th and U, but not for the isotope ratios. To use the same methodology as that shown before we used activity ratios instead of isotope ratios. In this way, the activity ratios obtained for the two analyzed aliquots were 0.004632±0.00026 and 0.004638±0.00015 for $^{235}U/^{238}U$, 1.031±0.016 and 1.042±0.010 for $^{234}U/^{238}U$, and 1.033±0.040 and 1.080±0.027 and for $^{230}Th/^{232}Th$.

3.2. Future developments.

The radiochemical setup described above is time-consuming, especially due to the use of low-temperature evaporations during the fluoride ions removal. This step consumes approximately 50% of the analytical time. The recent incorporation to our lab of a microwave driven evaporator (Milestone MMR-8) could substantially reduce the analytical time whilst minimizing potential evaporations of analytes (Maichin et al.,

2000). Additionally, author's experience with the ICP-MS/MS system suggests that under normal conditions the sensitivity of the instrument drops by a factor 2-3 when exchanging from single quad mode to MS/MS mode. Recent tests suggested that second lenses re-tuning after 24h stabilization time could improve the sensitivity up to (with ARIDUS II) 250 cps/ppt in the range of masses of the analytes here described. This fact suggests that the sample mass could be easily reduced by a factor ×2, thereby making the radiochemical separation easier.

3.3. U and Th isotopes in kaolinitic samples.

The interpretation of the activity ratios should be based on the knowledge of the geochemical differences between U and Th and the mechanisms driving their removal and accumulation. In oxic environments, U generally exists as the highly soluble uranyl species UO_2^{2+}, and this solubility is enhanced by U ability to form complexes with carbonates, oxalates, phosphates, hydroxides and organic ligands (Chabaux et al., 2008). However, it can be removed from the water column following salinity changes (e.g., estuary systems) or at sub-oxic or reducing environments (Ivanovich and Harmon, 1992). ^{238}U decays to ^{234}U through two short-lived ($T_{1/2}$ < 1 month) daughters hence generating continuously the grand-daughter inside the water mass. Moreover, U isotopes are continuously leached in weathered rocks; the alpha recoil produces a weakening of binding of ^{234}U inside the mineral lattice relative to ^{238}U and, as a consequence, water masses are commonly slightly enriched in the grand-daughter nuclide (Ivanovich and Harmon, 1992). For example, $^{234}U/^{238}U$ activity ratios in contemporary seawater in the Atlantic and Mediterranean basins are quite homogeneous both geographically and with depth inside the water column, ~1.14 (Koide and Goldberg, 1965). Much higher values, up to 2.0, have been recorded in various large rivers on the world, and values much higher than those can be found in underground water masses (Dunk et al., 2002).

On the other hand, Th is a particle-reactive element having less solubility than uranium in water. As a consequence, ^{230}Th produced by ^{234}U decay in the water column is rapidly scavenged in the presence of settling particles in water, especially in environments with high particle fluxes such as coastal environments, leading to $^{230}Th/^{234}U$ activity ratios below unity in the dissolved phase of the water column, and higher than unity in the particulate or colloidal phases (McKee, 2008). In the same way, the lower solubility of thorium relative to uranium leads to $^{230}Th/^{234}U$ activity ratios higher than unity in weathered rocks (Francois et al., 2004). The half-lives of the involved radionuclides are very different (75.4 and 246 ky for ^{230}Th and ^{234}U respectively). Thus, if the leaching of a rock stops, the excess of ^{230}Th would decay faster than ^{234}U. Under these conditions, once they reach again secular equilibrium, both of them decay with the half-life of the parent. The case of ^{232}Th is different, as its geochemical properties are the same as ^{230}Th, and it is the parent of its own decay series.

Uranium and thorium concentrations in the analyzed samples are shown in Table 3. Table 3 also includes several isotope ratios ($^{234}U/^{238}U$, $^{230}Th/^{238}U$ and $^{238}U/^{232}Th$) commonly used in the analysis of weathering profiles, e.g. Chabaux et al. (2003). In this case, activity ratios instead of atom number ratios are used.

While several of the uranium and thorium concentrations were near the world-wide average and West Europe for topsoil, (~ 3 µg/g and 6 µg/g, respectively) (United Nations Scientific Committee on the Effects of Atomic Radiation, 2000), several samples show concentrations up to four times higher than these averages, and within the ranges published by (Viruthagiri et al., 2013) for kaolin and bauxite samples from Egypt. Furthermore, $^{238}U/^{232}Th$ activity ratios covered the range 0.3-6.0, most of them quite far from the typical value of the contemporary range for Atlantic shelf (0.6-0.8) (Henderson and Anderson, 2003); this fact suggests that U and Th concentrations in the samples depend on the lithology, the original environmental conditions and the historic evolution.

Two of the above-mentioned isotope ratios have been used in Figure 4 ($^{234}U/^{238}U$ *vs.* $^{230}Th/^{238}U$). The horizontal and vertical lines at isotope ratios = 1.0 represent a situation of secular equilibrium between the isotopes in numerator and denominator. Likewise, the line with slope 1.0 represents the situation where ^{234}U and its daughter ^{230}Th are under secular equilibrium. The zero hypothesis in this study establishes that if the samples formed dozens of million years ago, and if they belong to formations behaving like closed systems (i.e., they did not suffer subsequent weathering or material accumulation), all of them should be located around the point where the three straight lines intersect. Note that this is the case for the two DBC CRM replicates where a significance level of 99% (i.e., k = 3) is used. It is easy to see that this was not the case for the samples here analyzed.

Furthermore, the subsector upper/left (noted as "IV" in the figure) should correspond to a situation mainly driven by U accumulation from a water mass; that would occur for example due to precipitation with settling organic/inorganic particles (the so-called "marine snow"), under reducing environments, etc., with $^{234}U/^{238}U$ higher than unity and $^{230}Th/^{238}U$ less than unity. The subsector lower/right (noted as "II" in the figure) should correspond in turn to a situation manly driven by U leaching, in that way that ^{234}U preferential leaching leads to $^{234}U/^{238}U$ less than unity and $^{230}Th/^{238}U$ higher than unity due to the lower thorium solubility (Chabaux et al., 2003). The subsectors marked as "I" and "III" are the so-called Forbidden Zones or Complex Zones. Should the samples being collected from a single scenario dominated by the combination of radioactive decay and either rock leaching or U accumulation, no samples would be located in those subsectors. Once again, this was not the case, and this fact suggests that for the greatest proportion of the studied samples no single scenario could be assumed for the settings they were collected from.

Bearing in mind that the rocks have been exposed in the surface under weathering conditions at least from Miocene to present and that the samples were collected from

different materials and different depths, the discussion about the different isotope ratios was established according to the subsectors in Figure 4 where the results are located.

3.3.1. Subsector I ("Complex zone").

This subsector includes sample FR-9, which is characterized for having the highest Th concentration, as well as both the highest $^{234}U/^{238}U$ and $^{230}Th/^{238}U$ activity ratios (1.115 ± 0.013 and 1.139 ± 0.019, respectively).

The activity ratio $^{234}U/^{238}U$ >1 may be due to a preferential ^{238}U leaching in comparison with ^{234}U. However, this process is quite unlikely since ^{234}U is more mobile owing to the destabilization of the structure during alpha recoil in the radioactive decay, as explained above. The other possibility is the accumulation of ^{234}U at a lower level after leaching from the surface soil. The process should be slow enough for the production of ^{230}Th in secular equilibrium with ^{234}U, which in turn, will produce an activity ratio $^{230}Th/^{238}U$ higher than unity. The weak enrichment in ^{230}Th in comparison with ^{234}U ($a_{Th\text{-}230}/a_{U\text{-}234}$=1.022) may be due to some ^{234}U is still leaching from this level. These results are consistent with sample FR-9, a lateritic claystone rich in iron oxy-hydroxides and kaolinite where the weathering processes continued developing slowly. Under these conditions, ^{238}U would remain mostly stable associated with iron oxy-hydroxides, while the weaker bounds of ^{234}U allowed its leaching to the lower level.

Finally, the low value of the $^{238}U/^{232}Th$ activity ratio is consistent with the alteration profile of a laterite, where a previous and continuous leaching removed selectively uranium, but not thorium.

3.3.2. Subsector II.

Rigorously speaking, there are no samples in this subsector, although sample EST-2 have mixing properties between subsectors II (leaching) and I (Complex Zone). The activity ratio $^{230}Th/^{238}U$ >1 suggests either (or both) ^{230}Th accumulation or ^{238}U leaching. On the other hand, the activity ratio $^{234}U/^{238}U$ corresponds to secular equilibrium, showing that no preferential leaching of ^{234}U *vs* ^{238}U. Therefore, a continuous leaching equally affecting both ^{234}U and ^{238}U is necessary to get their secular equilibrium and the enrichment in ^{230}Th. How this leaching can equally affect both uranium isotopes can be related with the characteristics of sample EST-2, a dark claystone rich in coal from the Escucha Formation. Although a preferential leaching of ^{234}U *vs* ^{238}U was expected, ^{234}U could either be adsorbed by coal or precipitated under reducing environment. The continuous weathering would also release ^{238}U, which would be equally adsorbed or precipitated as before. After this, both U isotopes would have the same ability to leach, while ^{230}Th were accumulating.

The high concentration of total Th and high activity of ^{232}Th is typical of high sedimentation rate environments after its transport with the colloidal phase (McKee, 2008), which, in turn, is consistent with the initial formation of the sample material.

3.3.3. Subsector III ("Complex zone").

This subsector includes samples F2Y and MV36AC (the sample MV36AR has mixing properties corresponding to subsectors III and IV, although it has been included in this subsection for the sake of simplicity). For these samples, $^{234}U/^{238}U$ <1.0 is consistent with leached profiles. However, a typical leaching profile would be coupled to $^{230}Th/^{238}U$ > 1.0 due to the solubility of Th lower than that of U, which is not ~~our~~ the studied case. Indeed, sample F2Y presents the lower $^{230}Th/^{238}U$ activity ratio among the analyzed samples. A Th leaching seems to be quite unlikely, since this element is immobile in comparison with U. Therefore, the other possibility is a strong accumulation of U (both ^{234}U and ^{238}U) in a lower level of a leaching profile. This process is consistent with sample F2Y, composed of pisolitic bauxite embedded in red clays filling karst cavities. Although the karstification was developed in the Lower Cretaceous, subsequent karst reactivation has developed kaolinization processes due to circulation of acid solutions in the upper part of the profile (Yuste et al., 2015), which, in turn, would involve the uranium accumulation in the lower level. These processes could have been developed during the Alpine orogeny in the Tertiary period, but previous works have suggested that they can have been acting up to present (La Iglesia and Ordóñez, 1990; Molina and Salas, 1993).

The very low $^{230}Th/^{238}U$ activity ratio suggests that a high accumulation of ^{238}U was happening. It is worth to note that ^{234}U would be accumulating at the same rate that ^{238}U, since both have the same properties. This should involve an activity ratio, at least, equal to or higher than 1, the last considering a higher leaching of ^{234}U from the upper level. However, ^{234}U produced from the decay of ^{238}U will have a higher mobility than ^{238}U, as explained above, causing an activity ratio lower than 1, as is the case here.

The total content in Th, which is not very high, is consistent with the parent rock: the limestone where the karst was developed. Moreover, at the lower level where the sample was collected, accumulation of more mobile elements, such as U, were happening, consistently with the high total content of uranium. On the contrary, the upper part of the profile should have the highest content in thorium.

Concerning sample MV36AC, which is mainly formed by red claystones, similar accumulation of both ^{234}U and ^{238}U could happen at a lower level of the profile, as explained above. The difference is a lower entrance of uranium causing a higher, but still quite low, $^{230}Th/^{238}U$ activity ratio than before. After that, the decay of ^{238}U would produce ^{234}U, which would leach at the same rate as before, as shown by their activity ratio.

The low activity ratio $^{238}U/^{232}Th$ (0.77 ±0.042) is due to the high total content in thorium, which again is consistent with the characteristics of the lithology (a claystone) and the affinity of thorium for clays (McKee, 2008). According to the process described, the total content in uranium is high in comparison with other samples.

Finally, sample MV36AR belongs to the same formation as MV36AC, but it corresponds to a sandstone, with a coarser grain size. In this case, the accumulation of both ^{234}U and ^{238}U is lower than before, but it still exists to produce an activity ratio $^{230}Th/^{238}U < 1$. One possibility for this lower accumulation can be related with the coarser grain size and the lower capacity for uranium retention. Under these conditions, ^{234}U (particularly that originated from ^{238}U radioactive decay) would easily leach leading to an activity ratio $^{234}U/^{238}U < 1$, which would not correspond with the secular equilibrium observed. However, a higher leaching capacity for ^{234}U is also expected from the upper level, which would compensate the loss leading to the secular equilibrium.

The total content of both U and Th are not high, consistent with the lithology and processes described. However, according to the higher accumulation of uranium *vs* thorium, the activity ratio $^{238}U/^{232}Th$ is some high in comparison with other samples.

3.3.4. Subsector IV.

As previously explained, this subsector corresponds to a single scenario of uranium accumulation and it comprises sample AR6. The isotope ratio $^{230}Th/^{238}U$ less than unity in sample AR6 suggests that the time spent from the last uranium accumulation has been not long enough for ^{234}U and ^{230}Th to reach secular equilibrium again (<450 ky). While this sample comes from a similar geological setting and geographical area as sample EST-2, both activity ratios are quite different, although $^{238}U/^{232}Th$ are very similar to each other. It is possible, therefore, that the rate of sedimentation was different for each of the sample sites (Ariño and Estercuel) with greater sediment accumulation at the second site (sample EST2 for Estercuel) (Francois et al., 2004).

4. Conclusions.

A method for the analysis of long-lived radionuclides of uranium and thorium in kaolinitic samples by ICP-MS/MS has been described. The method is based on the full digestion of ≥ 0.25 g sample and the subsequent preparation of the solution for the sequential separation of uranium and thorium using extraction chromatography UTEVA® resins. The results show that the full digestion of kaolinitic samples requires longer digestion times than contemporary sediment samples, as expected. For both analytes, no relevant losses were produced neither during digestion nor evaporations. Small losses were produced during the Fe hydroxides co-precipitation, and certain losses could be attributed to an incomplete extraction of uranium and thorium from the resin into separate solutions. Total chemical yields were quantitative, as they can be estimated in 85% for uranium and around 80% for thorium before its subsequent purification using a TEVA® extraction chromatography resin. The crosstalk between

uranium and thorium resulted to be nearly negligible, hence the thorium fraction purification step was subsequently removed because it was unnecessary and resulted also in certain Th yield losses.

The application of the methodology, described above, to kaolinitic samples from the Iberian range allowed the use of $^{234}U/^{238}U$, $^{230}Th/^{238}U$ and $^{238}U/^{232}Th$ for the characterization of their recent time evolution. The activity ratios $^{230}Th/^{238}U$ <1 were related with accumulation of both ^{234}U and ^{238}U in the lower level of the profiles after leaching from the upper level. The activity ratios $^{230}Th/^{238}U$ >1 were related to leaching profiles. The activity ratio $^{234}U/^{238}U$ show the relative mobility of both isotopes. In sandstones, ^{234}U was easily mobile, particularly after its formation from ^{238}U radioactive decay, but it can be retained under reducing conditions associated with coal. Total content in thorium was related to ^{232}Th and depends on the lithology, the original environment and the historic evolution. The concentration increased from limestone, to sandstone and claystone. Laterites and bauxites accumulated thorium at the upper level were leaching processes happen, but the content is not necessarily high at lower levels.

7. Acknowledgments.

This research was funded by the Spanish Ministerio de Educación y Ciencia (CGL2013-46169-C2-1-P and CGL2013-46169-C2-2-P) and the contract of Domingo Martín granted by the V Plan Propio de Investigación de la Universidad de Sevilla. The authors want to acknowledge Prof. E. Alonso and Dr. A. Calleja (Servicios de Radioisótopos, Universidad de Sevilla) for facilitating access to the laboratory facilities and their kind help during the running of analyses. Authors are grateful to Emilio Galán for his teachings on the study of kaolins and applied mineralogy in general. He has been a teacher for us and a model to follow in life and as a researcher (Figure 5).

6. References.

Aguilar, M.J., Ramírez del Pozo, J., R.O., 1971. Algunas precisiones sobre la sedimentación y paleoecología del Cretácico inferior en la zona de Utrillas-Villarroya de los Pinares (Teruel). Estud. Geológicos 497–512.

Balcaen, L., Bolea-Fernandez, E., Resano, M., Vanhaecke, F., 2015. Inductively coupled plasma – Tandem mass spectrometry (ICP-MS/MS): A powerful and universal tool for the interference-free determination of (ultra)trace elements – A tutorial review. Anal. Chim. Acta 894, 7–19. https://doi.org/10.1016/j.aca.2015.08.053

Bardossy, G., 1982. Karst Bauxites. Bauxite Deposits on Carbonate Rocks, Developments in Economic Geology. Elsevier, Amsterdam. Elsevier, 443 pp. https://doi.org/10.1016/0016-7061(83)90006-x

Bauluz, B., Yuste, A., Mayayo, M.J., Canudo, J.I., 2014. Early kaolinization of detrital Weald facies in the Galve Sub-basin (Central Iberian Chain, north-east Spain) and its relationship to palaeoclimate. Cretac. Res. https://doi.org/10.1016/j.cretres.2014.03.014

640 Beyer, S.R., Hiatt, E.E., Kyser, K., Dalrymple, R.W., Pettman, C., 2011. Hydrogeology,
641 sequence stratigraphy and diagenesis in the Paleoproterozoic western Thelon Basin:
642 Influences on unconformity-related uranium mineralization. Precambrian Res. 187,
643 293–312. https://doi.org/10.1016/j.precamres.2011.03.012

644 Canérot, J., Cugny, P., Pardo, G., Salas, R., Villena, J., 1982. Ibérica central y
645 Maestrazgo., in: García, A. (Ed.), El Cretácico de España. Universidad
646 Complutense de Madrid, Madrid, pp. 273–344.

647 Canudo, J.I., Gasca, J.M., Moreno-Azanza, M., Aurell, M., 2012. New information
648 about the stratigraphic position and age of the sauropod Aragosaurus ischiaticus
649 from the Early Cretaceous of the Iberian Peninsula. Geol. Mag.
650 https://doi.org/10.1017/S0016756811000732

651 Carenas, B. 1987. El Cretácico medio de la región de Liria-Ademuz (Valencia). Ph.D.
652 Th. Diss. Univ. Complutense de Madrid, 868 p.

653 Casas Sainz, A.M., Faccena, C. 2001. Tertiary compressional deformation of the Iberian
654 Plate. Terra Nov, 13, 281-288. https://doi.org/10.1046/j.1365-3121.2001.00355.x

655 Carter, H.E., Warwick, P., Cobb, J., Longworth, G., 1999. Determination of uranium
656 and thorium in geological materials using extraction chromatography. Analyst 124,
657 271–274. https://doi.org/10.1039/a809781j

658 Chabaux, F., Bourdon, B., Riotte, J., 2008. Chapter 3 U-Series Geochemistry in
659 Weathering Profiles, River Waters and Lakes. Radioact. Environ.
660 https://doi.org/10.1016/S1569-4860(07)00003-4

661 Chabaux, F., Riotte, J., Dequincey, O., 2003. U-Th-Ra fractionation during weathering
662 and river transport, in: Uranium-Series Geochemistry.
663 https://doi.org/10.2113/0520533

664 ÇIflikli, M., ÇIftçi, E., Bayhan, H., 2013. Alteration of glassy volcanic rocks to Naand
665 Ca-smectites in the Neogene basin of Manisa, western Anatolia, Turkey. Clay
666 Miner. 48, 513–527. https://doi.org/10.1180/claymin.2013.048.3.08

667 Clauer, N., Fallick, A.E., Galán, E., Aparicio, P., Miras, A., Fernández-Caliani, J.C.,
668 Aubert, A., 2015. Stable isotope constraints on the origin of kaolin deposits from
669 Variscan granitoids of Galicia (NW Spain). Chem. Geol. 417, 90–101.
670 https://doi.org/10.1016/j.chemgeo.2015.09.022

671 Crawford, S.E., Liber, K., 2015. Effects of clay minerals and organic matter in
672 formulated sediments on the bioavailability of sediment-associated uranium to the
673 freshwater midge, Chironomus dilutus. Sci. Total Environ. 532, 821–830.
674 https://doi.org/10.1016/j.scitotenv.2015.05.116

675 Dill, H.G., 2017. Residual clay deposits on basement rocks: The impact of climate and
676 the geological setting on supergene argillitization in the Bohemian Massif (Central
677 Europe) and across the globe. Earth-Science Rev. 165, 1–58.
678 https://doi.org/10.1016/j.earscirev.2016.12.004

679 Dunk, R., Mills, R., Jenkins, W., 2002. A reevaluation of the oceanic uranium budget
680 for the Holocene. Chem. Geol. 190, 45–67. https://doi.org/10.1016/S0009-

2541(02)00110-9

El-Dine, N.W., Sroor, A., El-Shershaby, A., El-Bahi, S.M., Ahmed, F., 2004. Radioactivity in local and imported kaolin types used in Egypt, Applied Radiation and Isotopes. https://doi.org/10.1016/j.apradiso.2003.09.006

Fernández-Caliani, J.C., Cantano, M., 2010. Intensive kaolinization during a lateritic weathering event in South-West Spain. Mineralogical and geochemical inferences from a relict paleosol. Catena. https://doi.org/10.1016/j.catena.2009.08.005

Fernández-Caliani, J.C., Galán, E., Aparicio, P., Miras, A., Márquez, M.G., 2010. Origin and geochemical evolution of the Nuevo Montecastelo kaolin deposit (Galicia, NW Spain). Appl. Clay Sci. 49, 91–97. https://doi.org/10.1016/j.clay.2010.06.006

Francois, R., Frank, M., Rutgers van der Loeff, M.M., Bacon, M.P., 2004. 230 Th normalization: An essential tool for interpreting sedimentary fluxes during the late Quaternary . Paleoceanography. https://doi.org/10.1029/2003pa000939

Galán, E., Aparicio, P., Fernández-Caliani, J.C., Miras, A., Márquez, M.G., Fallick, A.E., Clauer, N., 2016. New insights on mineralogy and genesis of kaolin deposits: The Burela kaolin deposit (Northwestern Spain). Appl. Clay Sci. 131, 14–26. https://doi.org/10.1016/j.clay.2015.11.015

García, A., Mas, R. (coord.), Segura, M., Carenas, B., García-Hidalgo, J.F., Gil, J., Alonso, A., Aurell, M., Bádenas, B., Benito, M.I., Meléndez, A., Salas, R. 2004. Segunda fase del post-rifting: Cretácico superior. In: Vera, J.A. (Ed.), Geología de España, SGE-IGME, Madrid, 510-522.

Giachetta, E., Molin, P., Scotti, V.N., Faccena, C. 2015. Plio-Quaternary uplift of the Iberian Chain (central–eastern Spain) from landscape evolution experiments and river profile modeling. Geomorphology, 246, 48-67. 10.1016/j.geomorph.2015.06.005

González López, J.M., Bauluz, B., Yuste, A., Mayayo, M.J., Fernández-Nieto, C., 2005. Mineralogical and trace element composition of clay-sized fractions from Albian siliciclastic rocks (Oliete Basin, NE Spain). Clay Miner. https://doi.org/10.1180/0009855054040193

Henderson, G.M., Anderson, R.F., 2003. The U-series toolbox for paleoceanography, in: Uranium-Series Geochemistry. https://doi.org/10.2113/0520493

Herranz, M., Lozano, J.C., Bolívar, J.P., García-Tenorio, R., 2015. Comparison of several methods for thorium-isotopes determination in Environmental and Industrial Samples, in: ENVIRA2015 International Conference on Environmental Radioactivity: New Challenges with New Technologies. 21–25 September. Thessaloniki, Greece.

Hou, X., Roos, P., 2008. Critical comparison of radiometric and mass spectrometric methods for the determination of radionuclides in environmental, biological and nuclear waste samples. Anal. Chim. Acta 608, 105–139. https://doi.org/10.1016/j.aca.2007.12.012

722 Ivanovich, M., Harmon, R.S., 1992. Uranium-series disequilibrium: applications to
723 earth, marine, and environmental sciences, 2nd edition. Uranium-series
724 disequilibrium Appl. to earth, Mar. Environ. Sci. 2nd Ed.
725 https://doi.org/10.1016/0009-2541(93)90082-T

726 Koide, M., Goldberg, E.D., 1965. Uranium-234/uranium-238 ratios in sea water. Prog.
727 Oceanogr. 3, 173–177. https://doi.org/10.1016/0079-6611(65)90016-9

728 La Iglesia, A. Ordóñez, S., 1990. Cristalinidad de caolinitas en yacimientos de bauxitas
729 cársticas del NE España. Bol. Soc. Esp. Mineral. 13: 81-90.

730 Lee, S.H., La Rosa, J., Gastaud, J., Povinec, P.P., 2005. The development of sequential
731 separation methods for the analysis of actinides in sediments and biological
732 materials using anion-exchange resins and extraction chromatography. J.
733 Radioanal. Nucl. Chem. 263, 419–425. https://doi.org/10.1007/s10967-005-0071-8

734 Lozano, J.C., 2012. Extracción de torio en muestras sólidas (In Spanish), in: VII
735 Jornadas Sobre Calidad En El Control de La Radiactividad Ambiental. Consejo de
736 Seguridad Nuclear, Madrid, pp. 182–190.

737 Maichin, B., Kettisch, P., Knapp, G., 2000. Investigation of microwave assisted drying
738 of samples and evaporation of aqueous solutions in trace element analysis.
739 Fresenius. J. Anal. Chem. https://doi.org/10.1007/s002160050006

740 Martin-Chivelet, J. (coord.), Berástegui, X., Rosales, I., Vilas, L., Vera, J.A., Caus, E.,
741 Gräffe, K.U., Segura, M., et al. 2002. Cretaceous. In: Gibbons, W., Moreno, T.
742 (Eds.), Geology of Spain, Geol. Soc., London, 255-293.

743 Mas, R. 1981. El Cretácico inferior de la región noroccidental de la provincia de
744 Valencia. Ph. D. Th. Diss. Univ. Complutense Madrid.

745 Mas, J.L.L., Villa, M., Hurtado, S., García-Tenorio, R., 2012. Determination of trace
746 element concentrations and stable lead, uranium and thorium isotope ratios by
747 quadrupole-ICP-MS in NORM and NORM-polluted sample leachates. J. Hazard.
748 Mater. 205–206, 198–207. https://doi.org/10.1016/j.jhazmat.2011.12.058

749 Masarik, J., 2009. Chapter 1 Origin and Distribution of Radionuclides in the
750 Continental Environment, Radioactivity in the Environment. Elsevier.
751 https://doi.org/10.1016/S1569-4860(09)01601-5

752 Maxwell, S.L., Culligan, B.K., 2006. Rapid column extraction method for actinides in
753 soil. J. Radioanal. Nucl. Chem. 270, 699–704. https://doi.org/10.1007/s10967-006-
754 0449-2

755 McKee, B.A., 2008. Chapter 6 U- and Th-Series Nuclides in Estuarine Environments.
756 Radioact. Environ. https://doi.org/10.1016/S1569-4860(07)00006-X

757 Molina, J., Salas, R., 1993. Bauxitas kársticas del Cretácico inferior en Fuenteespalda
758 (provincia de Teruel): estratígrafía, origen y paleogeografía. Cuad. Geol. Ibérica,
759 17, 207-230.

760 Navarrete, R., Rodríguez-López, J.P., Liesa, C.L., Soria, A.R., Veloso, F. de M.L.,
761 2013. Changing physiography of rift basins as a control on the evolution of mixed

762 siliciclastic-carbonate back-barrier systems (Barremian Iberian Basin, Spain).
763 Sediment. Geol. https://doi.org/10.1016/j.sedgeo.2013.02.003

764 Ohno, T., Muramatsu, Y., Shikamori, Y., Toyama, C., Okabe, N., Matsuzaki, H., 2013.
765 Determination of ultratrace 129I in soil samples by Triple Quadrupole ICP-MS and
766 its application to Fukushima soil samples. J. Anal. At. Spectrom. 28.
767 https://doi.org/10.1039/c3ja50121c

768 Oliveira, J.M., Carvalho, F.P., 2006. Sequential extraction procedure for determination
769 of uranium, thorium, radium, lead and polonium radionuclides by alpha
770 spectrometry in environmental samples. Czechoslov. J. Phys. 56, 545–555.
771 https://doi.org/10.1007/s10582-006-0548-x

772 Osmond, J.K., Ivanovich, M., 1992. Uranium-series mobilization and surface
773 hydrology, in: Uranium Series Disequilibrium: Application to the Earth, Marine
774 and Environmental Sciences. pp. 259–288.

775 Pellenard, P., Deconinck, J.-F., 2006. Mineralogical variability of Callovo-Oxfordian
776 clays from the Paris Basin and the Subalpine Basin. Comptes Rendus - Geosci. 338.
777 https://doi.org/10.1016/j.crte.2006.05.008

778 Pham, M.K., Sánchez-Cabeza, J.A., Povinec, P.P., 2005. Report on the Worldwide
779 Intercomparison Exercise IAEA-385.

780 Pham, M.K., Sanchez-Cabeza, J.A., Povinec, P.P., Andor, K., Arnold, D., Benmansour,
781 M., et al. 2008. A new Certified Reference Material for radionuclides in Irish sea
782 sediment (IAEA-385). Appl. Radiat. Isot. 66.
783 https://doi.org/10.1016/j.apradiso.2007.10.020

784 Querol, X., Salas, R., Pardo, G., Ardevol, L., 1992. Albian coal-bearing deposits of the
785 Iberian Range in Northeastern Spain. Spec. Pap. Geol. Soc. Am.
786 https://doi.org/10.1130/SPE267-p193

787 Raucsik, B., Varga, A., 2008. Climato-environmental controls on clay mineralogy of the
788 Hettangian-Bajocian successions of the Mecsek Mountains, Hungary: An evidence
789 for extreme continental weathering during the early Toarcian oceanic anoxic event.
790 Palaeogeogr. Palaeoclimatol. Palaeoecol. 265.
791 https://doi.org/10.1016/j.palaeo.2008.02.004

792 Richland, W., Lundstrom, C., Turekian, K.K., 2003. Uranium – Series Geochemistry.
793 Rev. Mineral. Geochemistry 52.

794 Rihs, S., Gontier, A., Lascar, E., Biehler, A., Turpault, M.P., 2017. Effect of organic
795 matter removal on U-series signal in clay minerals. Appl. Clay Sci, 147, 128-136
796 https://doi.org/10.1016/j.clay.2017.07.016

797 Ruffell, A., McKinley, J.M., Worden, R.H., 2002. Comparison of clay mineral
798 stratigraphy to other proxy palaeoclimate indicators in the Mesozoic of NW
799 Europe. Philos. Trans. R. Soc. A Math. Phys. Eng. Sci. 360.
800 https://doi.org/10.1098/rsta.2001.0961

801 Ruiz-Omeñaca, J.I., Canudo, J.I., Aurell, M., Bádenas, B., Barco, J.L., Cuenca-Bescós,
802 G., Ipas, J., 2004. Estado de las investigaciones sobre los vertebrados del Jurasico
803 superior y cretacico inferior de Galve (Teruel). Estud. Geol. Vol 60, No 3-6

804 Salas, R. 1987. El Malm y el Cretaci inferior entre el Massis de Garraf i la Serra
805 d'Espadà. PhD. Th. Diss. University of Barcelona.

806 Salas, R., 1989. Evolución estratigráfica secuencial y tipos de plataformas de carbonatos
807 del intervalo Oxfordiense-Berriasiense en las cordilleras ibérica oriental y costero
808 catalana meridional. Cuad. Geol. Ibérica 13, 121-127.

809 Salas, R., Casas, A., 1993. Mesozoic extensional tectonics, stratigraphy and crustal
810 evolution during the Alpine cycle of the eastern Iberian basin. Tectonophysics.
811 https://doi.org/10.1016/0040-1951(93)90213-4

812 Salas, R., Martín-Closas, C., Querol, X., Guimerà, J., Roca, E., 1995. Evolución
813 tectonosedimentaria de las cuencas del Maestrazgo y Aliaga - Penyagolosa durante
814 el Cretácico inferior. El Cretácico Infer. del Nord. Iberia 15–94.

815 Salas, R., Guimerà, J., Mas, R., Martín-Closas, C, Meléndez, A., Alonso, A. 2001.
816 Evolution of the Mesozoic central Iberian Rift System and is Cainozoic inversión
817 (Iberian Chain). In: Ziegler, P.A., Cavazza, W., Robertson, A.H.F., Carasquin-
818 Soleau, S. (Eds.), Peri-Tethys Memoir 6: Peri-Tethyan Rift/Wrench Basins and
819 Passive Margins. Mém. Mus. Natn. Hist. nat, 186, 145-185.

820 Soria, A.R., 1997. La sedimentación en las cuencas marginales del surco ibérico durante
821 el Cretácico inferior y su control estructural. Universidad de Zaragoza.

822 Taylor, S.R. and McLennan, S.M., 1985. The Continental Crust: Its Composition and
823 Evolution. Blackwell Scientific Publications, Oxford, 1985.
824 doi.org/10.1002/gj.3350210116

825 United Nations Scientific Committee on the Effects of Atomic Radiation, 2000. Annex
826 B. Exposures from natural radiation sources. Unscear 2000 Rep. 1, 74.

827 Van Wees, J.D., Arche, A., Beijdorff, C.G., López-Gómez, J., Cloetingh, S.A.P.L.,
828 1998. Temporal and spatial variations in tectonic subsidence in the Iberian Basin
829 (eastern Spain): Inferences from automated forward modelling of high-resolution
830 stratigraphy (Permian-Mesozoic). Tectonophysics. https://doi.org/10.1016/S0040-
831 1951(98)00244-3

832 Viruthagiri, G., Rajamannan, B., Suresh Jawahar, K., 2013. Radioactivity and
833 associated radiation hazards in ceramic raw materials and end products. Radiat.
834 Prot. Dosimetry 157, 383–391. https://doi.org/10.1093/rpd/nct149

835 Wyse, E.J., Lee, S.H., La Rosa, J., Povinec, P., de Mora, S.J., 2001. ICP-sector field
836 mass spectrometry analysis of plutonium isotopes: recognizing and resolving
837 potential interferences. J. Anal. At. Spectrom. 16, 1107–1111.
838 https://doi.org/10.1039/b102936n

839 Yuste, A., Bauluz, B., Mayayo, M.J., 2015. Genesis and mineral transformations in
840 Lower Cretaceous karst bauxites (NE Spain): Climatic influence and superimposed
841 processes. Geol. J. 50, 839–857. https://doi.org/10.1002/gj.2604

842 Zheng, J., Yamada, M., 2006. Determination of U isotope ratios in sediments using
843 ICP-QMS after sample cleanup with anion-exchange and extraction
844 chromatography. Talanta 68, 932–939.
845 https://doi.org/10.1016/j.talanta.2005.06.065

TABLE AND FIGURE CAPTIONS

Table 1: Summary of the measurement conditions for multi-element concentrations (left) and isotope analyses (right).

Table 2: Chemical yields obtained for U and Th in different parts of the process (sample IAEA-385). [1]: Solution obtained after microwave digestion, including rinsing of liners. [2]: After evaporating to almost dryness (×3). [3]: Supernatant after $Fe(OH)_2$ precipitation. [4]: Mixing of sample loading onto UTEVA column, washing and exchanging resin form to chloride form. [5]: Solution obtained after collecting the uranium fraction and exchanging sample matrix to 1% HNO_3. [6]: Th fraction after evaporating to almost dryness and recovery with 9M HCl, before TEVA resin. [7]: Th fraction after TEVA resin, evaporation to almost dryness and exchanging sample matrix to 1% HNO_3. [a, b]: Chemical yield (%) for U and Th, respectively. [c]: Ratio of count rate obtained in the procedure blank to the average of count rates obtained for replicates 1-4 of this step, expressed in terms of %.

Table 3: Concentrations of U and Th found by ID-ICP-MS/MS in the kaolinitic samples referred in the text. Uncertainties correspond to k=1. a_i/a_j corresponds to the activity concentration ratio between isotopes i and j.

Figure 1: Geographical location and geological setting of the samples collection points. Modified from Bauluz et al., 2014. The sampled sections are located with stars.

Figure 2: Schematic diagram of the separation procedure tested in this work. The aliquots taken for the sake of chemical yield calculation are numbered from (1) to (7).

Figure 3: Normalized results (uranium and thorium isotope ratios and element concentrations) obtained for the certified reference sample and a replicate of one of the samples described in the text.

Figure 4: $^{234}U/^{238}U$ vs. $^{230}Th/^{238}U$ activity ratios diagram. The subsectors marked as (I) and (III) are the so-called complex or forbidden zones, where no sample would be expected if the samples proceed from a simple leaching + U accumulation + radioactive decay scenario. Dotted lines show secular equilibrium between isotope ratios. Solid line show secular equilibrium between ^{234}U and ^{230}Th.

Figure 5: Prof Emilio Galán with Prof. Haydn Murray during a kaolin field trip in Galicia (Spain) in 2005.

883

884

Multi-element analysis (CFlow 400)		Isotope analysis (Aridus II)	
Mode	Single quad	**Mode**	MS/MS ("*On mass*")
Reaction cell	He, 4 mL/min	**Reaction cell**	Off
Peaks per mass	3	**Peaks per mass**	1
Internal standard	^{103}Rh, ^{209}Bi	**Dwell time (ms)**	232, 238: 0.3
Dwell time (ms)	103, 209: 3 232, 238: 15		235, 236: 2
			229, 234: 10
			230: 12.5
Number of sweeps	100	**Number of sweeps**	1000
Replicates	3	**Replicates**	5
Carrier	1.1 L/min	**Sweep gas (Ar)**	5.2 L/min
		N_2 flow rate	4 mL/min

885 Table 1: Summary of the measurement conditions for multi-element concentrations
886 (left) and isotope analyses (right).

887

888

Solution 1[1]	Replicate	Y_U (%)[a]	Y_{Th} (%)[b]	Solution 5[5]	Replicate	Y_U (%)[a]	Y_{Th} (%)[b]
	1	103.1 ± 2.4	98.4 ± 1.9		1	99.8 ± 3.9	0.294 ± 0.014
	2	101.6 ± 2.2	101.2 ± 2.1		2	86.2 ± 7.3	0.219 ± 0.018
	3	99.6 ± 2.1	101.3 ± 2.2		3	70.0 ± 2.7	6.96 ± 0.17
	4	102.4 ± 2.4	98.7 ± 1.8		4	106.0 ± 8.9	0.880 ± 0.067
	B / Avg (%)[c]	0.62 ± 0.43	1.4 ± 1.2		B / Avg (%)[c]	8	10
Solution 2[2]	**Replicate**	**Y_U (%)[a]**	**Y_{Th} (%)[b]**	**Solution 6[6]**	**Replicate**	**Y_U (%)[a]**	**Y_{Th} (%)[b]**
	1	102.1 ± 1.2	96.6 ± 1.3		1	1.548 ± 0.064	74.6 ± 2.0
	2	100.8 ± 1.2	102.1 ± 1.5		2	N.M.	
	3	101.5 ± 1.1	103.0 ± 1.6		3	0.924 ± 0.096	82.4 ± 6.5
	4	100.4 ± 1.2	97.4 ± 1.4		4	0.927 ± 0.057	88.3 ± 2.2
	B / Avg (%)[c]	1.12 ± 0.43	1.4 ± 1.2		B / Avg (%)[c]	8	0.11
Solution 3[3]	**Replicate**	**Y_U (%)[a]**	**Y_{Th} (%)[b]**	**Solution 7[7]**	**Replicate**	**Y_U (%)[a]**	**Y_{Th} (%)[b]**
	1	1.70 ± 0.23	0.067 ± 0.012		1	0.0299 ± 0.0014	68.4 ± 2.3
	2	6.51 ± 0.32	0.0803 ± 0.0084		2	N.M.	
	3	7.4 ± 1.1	0.171 ± 0.026		3	0.0453 ± 0.0038	82.2 ± 6.9
	4	0.307 ± 0.032	0.0158 ± 0.0021		4	0.0216 ± 0.0034	72.8 ± 9.7
	B / Avg (%)[c]	48	12		B / Avg (%)[c]	129	0.056
Solution 4[4]	**Replicate**	**Y_U (%)[a]**	**Y_{Th} (%)[b]**				
	1	0.280 ± 0.021	1.323 ± 0.056				
	2	0.367 ± 0.024	1.737 ± 0.091				
	3	0.1122 ± 0.0090	0.361 ± 0.021				
	4	0.332 ± 0.050	1.87 ± 0.24				
	B / Avg (%)[c]	32	4				

Table 2: Chemical yields obtained for U and Th in different parts of the process (sample IAEA-385). [1]: Solution obtained after microwave digestion, including rinsing of liners. [2]: After evaporating to almost dryness (×3). [3]: Supernatant after $Fe(OH)_2$ precipitation. [4]: Mixing of sample loading onto UTEVA column, washing and exchanging resin form to chloride form. [5]: Solution obtained after collecting the uranium fraction and exchanging sample matrix to 1% HNO_3. [6]: Th fraction after evaporating to almost dryness and recovery with 9M HCl, before TEVA resin. [7]: Th fraction after TEVA resin, evaporation to almost dryness and exchanging sample matrix to 1% HNO_3. [a, b]: Chemical yield (%) for U and Th, respectively. [c]: Ratio of count rate obtained in the procedure blank to the average of count rates obtained for replicates 1-4 of this step, expressed in terms of %.

Sample	[U] (μg/g)	[Th] (μg/g)	$a_{U\text{-}234}/a_{U\text{-}238}$	$a_{Th\text{-}230}/a_{U\text{-}238}$	$a_{U\text{-}238}/a_{Th\text{-}232}$
F2Y	15.99 ± 0.33	8.21 ± 0.38	0.761 ±0.018	0.135 ±0.003	5.97 ±0.30
FR-9 2 μm	3.076 ± 0.051	31.48 ± 0.73	1.115 ±0.013	1.139 ±0.019	0.300 ±0.009
MV36AR 2 μm	3.674 ± 0.091	6.89 ± 0.13	0.997 ±0.027	0.874 ±0.022	1.635 ±0.051
MV36AC 2 μm	5.25 ± 0.18	20.91 ± 0.89	0.776 ±0.009	0.622 ±0.021	0.770 ±0.042
AR6	3.413 ± 0.058	7.86 ± 0.38	1.103 ±0.019	0.614 ±0.011	1.304 ±0.067
EST-2	12.00 ± 0.24	20.03 ± 0.50	1.003 ±0.012	1.113 ±0.023	1.470 ±0.042

Table 3: Concentrations of U and Th found by ID-ICP-MS/MS in the kaolinitic samples referred in the text. Uncertainties correspond to k=1. a_i/a_j corresponds to the activity concentration ratio between isotopes i and j.

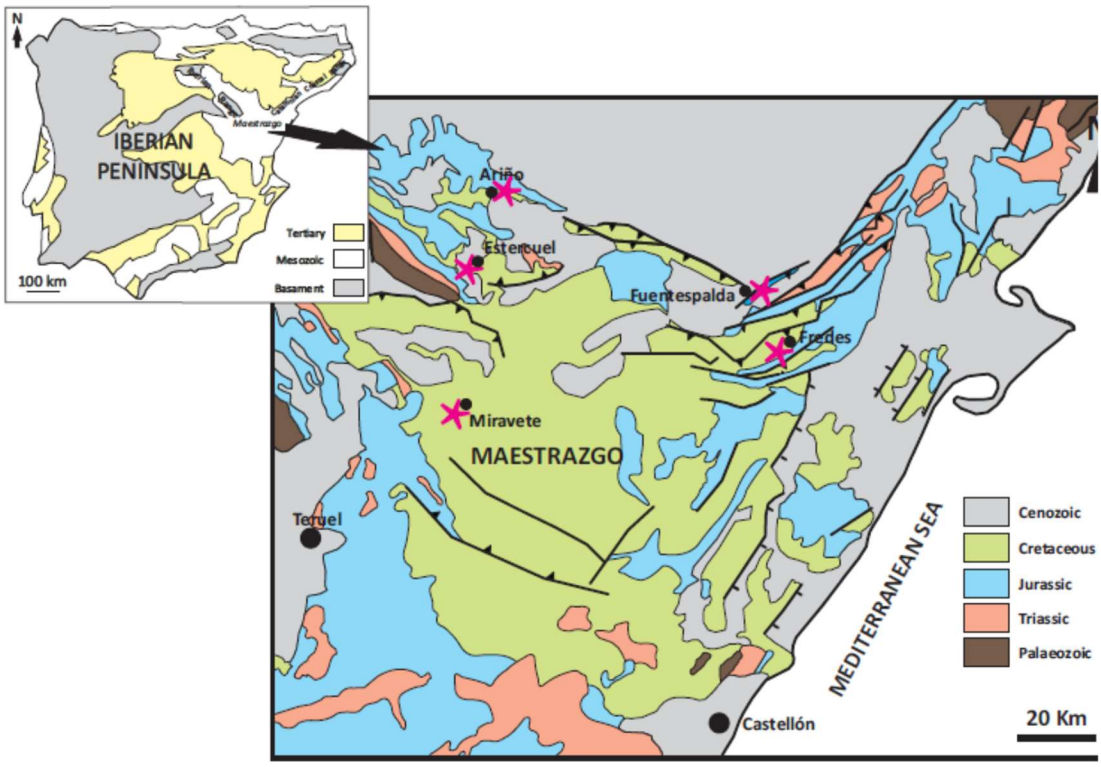

Fig. 1: Geographical location and geological setting of the samples collection points. Modified from Bauluz et al., 2014. The sampled sections are located with stars.

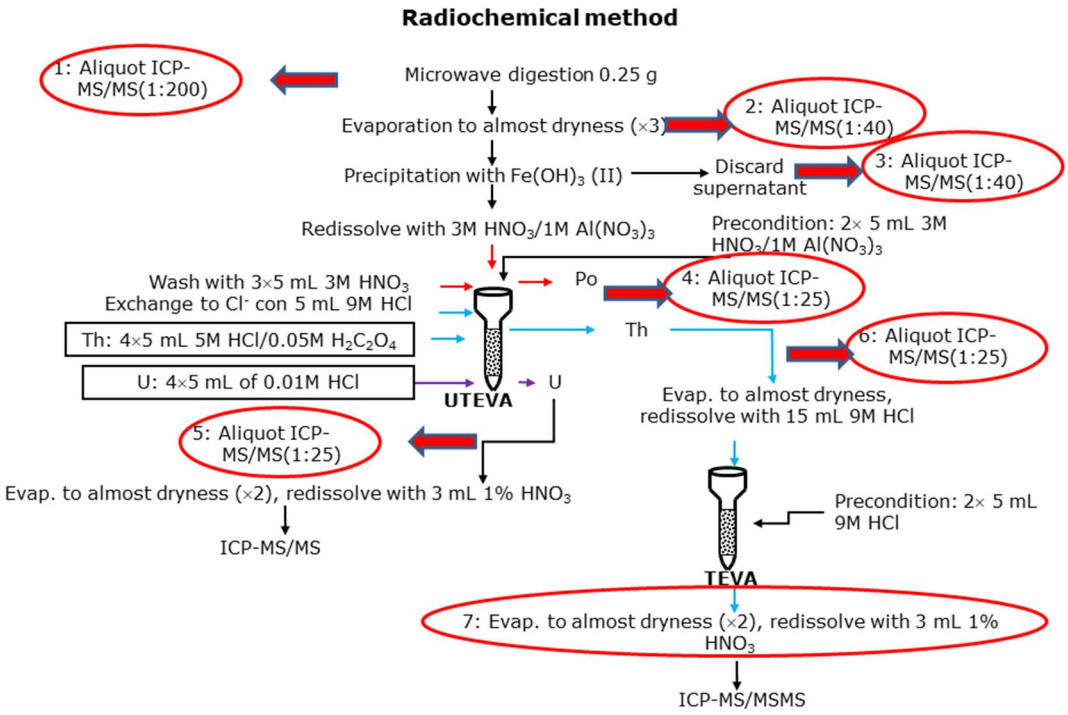

Fig. 2: Schematic diagram of the separation procedure tested in this work. The aliquots taken for the sake of chemical yield calculation are numbered from (1) to (7).

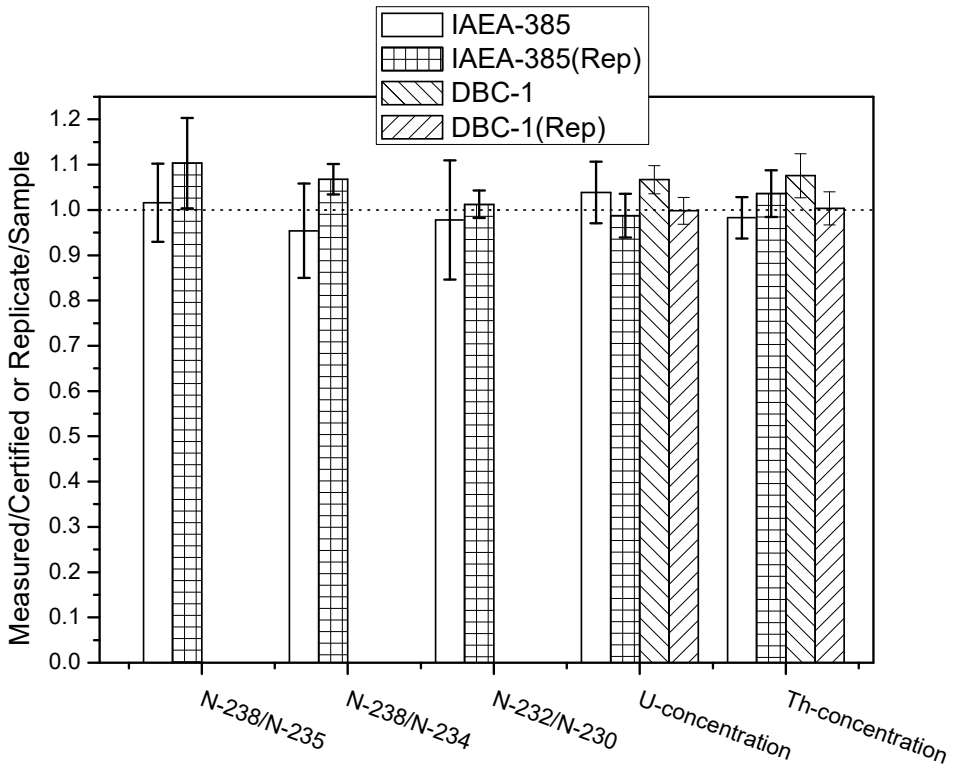

Fig. 3: Normalized results (uranium and thorium isotope ratios and element concentrations) obtained for the certified reference sample and a replicate of one of the samples described in the text.

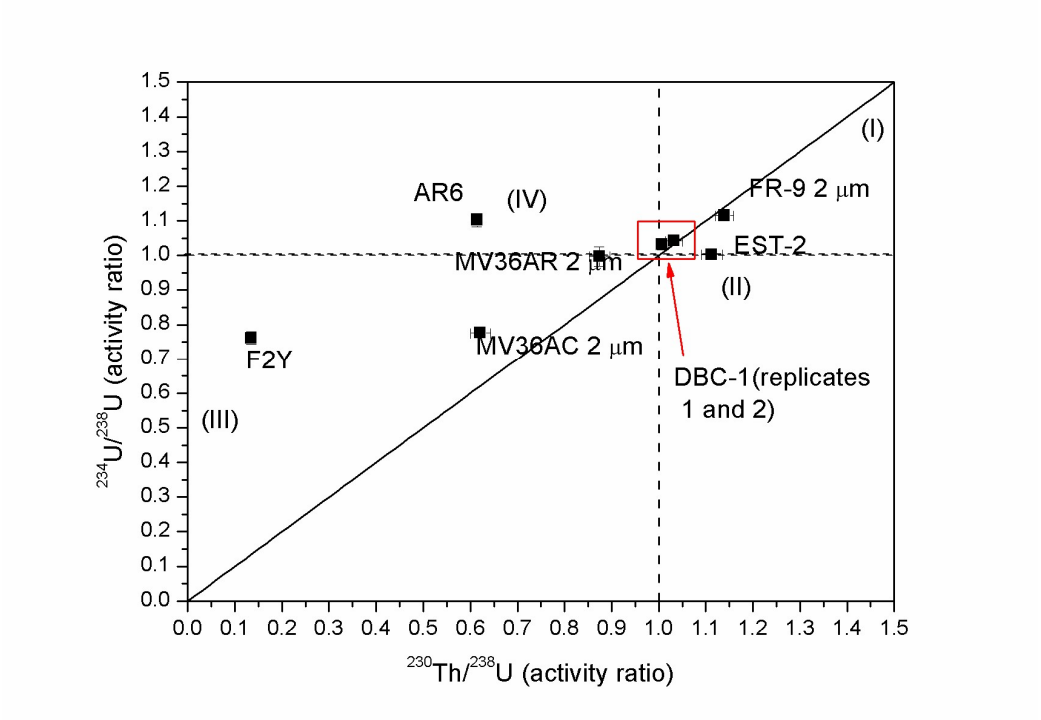

Figure 4: $^{234}U/^{238}U$ vs. $^{230}Th/^{238}U$ activity ratios diagram. The subsectors marked as (I) and (III) are the so-called complex or forbidden zones, where no sample would be expected if the samples proceed from a simple leaching + U accumulation + radioactive decay scenario. Dotted lines show secular equilibrium between isotope ratios. Solid line show secular equilibrium between ^{234}U and ^{230}Th.

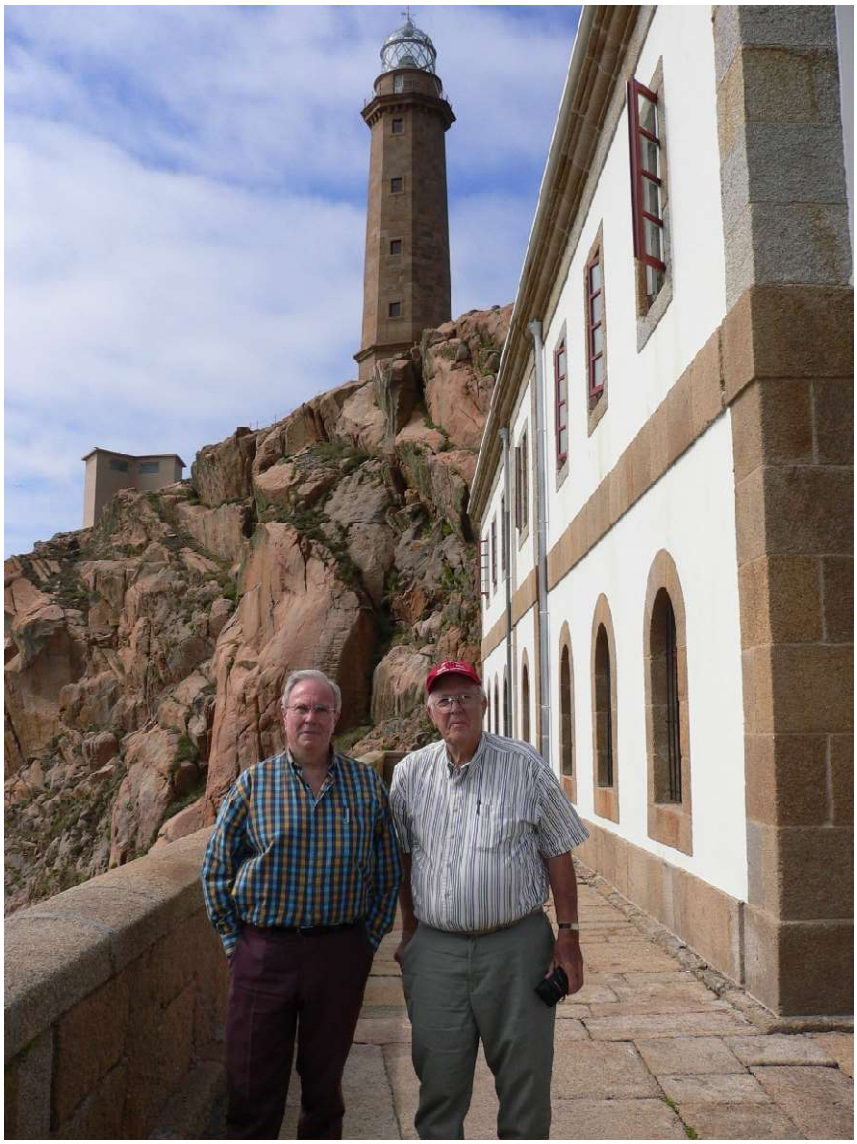

Figure 5: Prof Emilio Galán with Prof. Haydn Murray during a kaolin field trip in Galicia (Spain) in 2005.

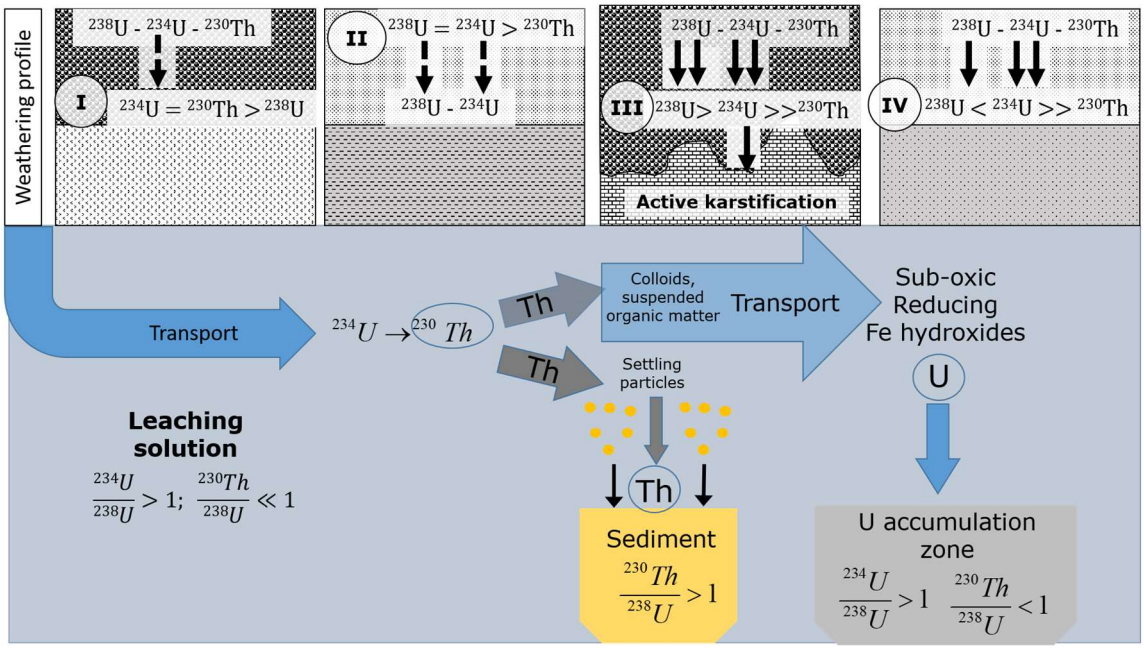

Graphical Abstract.